ACS OMEGA

Article

Cite This: ACS Omega 2019, 4, 14699−14713

http://pubs.acs.org/journal/acsodf

Evaluation of Cu/SAPO-34 Catalysts Prepared by Solid-State and Liquid Ion-Exchange Methods for NO_x Removal by NH_3-SCR

Maitane Urrutxua, Beñat Pereda-Ayo, Unai De-La-Torre, and Juan R. González-Velasco*

Department of Chemical Engineering, Faculty of Science and Technology, University of the Basque Country UPV/EHU, Barrio Sarriena s/n, 48940 Leioa, Bizkaia, Spain

Supporting Information

ABSTRACT: Cu/SAPO-34 catalysts are prepared using solid-state ion exchange (SSIE) and liquid ion exchange (LIE). SSIE is conducted by calcining a physical mixture of H-SAPO-34 zeolite and CuO nanoparticles at elevated temperatures (500−800 °C). The conventional LIE method is conducted by exchanging Na-SAPO-34 with $Cu(COOCH_3)_2$ aqueous solution with a final calcination step at 500 °C. Catalysts were fully characterized, focusing on Cu species identification. The NH_3-SCR activity is evaluated for NO_x removal. Cu/SAPO-34 catalysts synthesized by SSIE at 700 °C achieved an optimal reaction rate, which was correlated with a higher proportion of Cu^{2+} ions. The activation energies of Cu/SAPO-34 catalysts prepared by SSIE and LIE with varying copper loadings are 32−38 and 42−47 kJ mol^{-1}, respectively. The SSIE catalysts achieve higher turnover frequency than LIE catalysts for a similar copper content, which decreases on increasing the copper loading. These results provide evidence that Cu ions exchanged into the Cu/SAPO-34 catalysts synthesized by SSIE present higher activity than those prepared by LIE for NO_x removal by NH_3-SCR.

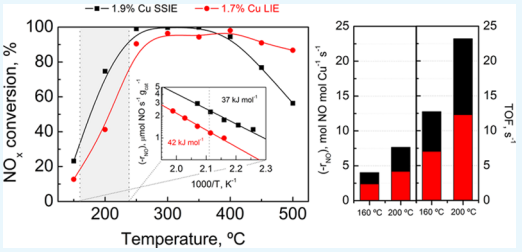

1. INTRODUCTION

In the last decades, diesel and lean-burn gasoline engines are attracting more and more attention as they provide better fuel economy and produce lower CO_2 emissions compared with conventional stoichiometric gasoline engines. However, the cleanup of diesel and lean-burn gasoline engine exhaust is more challenging, specifically regarding NO_x removal, due to the distinctly oxidant environment. Under these operating conditions, three-way catalyst are not efficient, and alternative catalytic strategies must be implemented to fulfill stringent emission standards. NO_x storage and reduction,[1] also denominated lean NO_x trap, and selective catalytic reduction (SCR)[2] are the preferred technologies to mitigate NO_x emission.

Selective catalytic reduction of NO_x by NH_3 (NH_3-SCR) is widely implemented for NO_x removal from heavy-duty diesel vehicles[3] and more recently has also been implemented for passenger cars.[4] NH_3-SCR operation requires a constant feeding of NH_3 to stoichiometrically reduce NO_x, running the operation at steady state. NH_3 is generated from the decomposition of urea solution injected into the exhaust gas upstream of the SCR catalyst.[5] There are three main reactions leading to NO_x reduction through NH_3-SCR: (i) standard SCR ($4NH_3 + 4NO + O_2 \rightarrow 4N_2 + 6H_2O$), (ii) fast SCR ($2NH_3 + NO + NO_2 \rightarrow 2N_2 + 3H_2O$), and (iii) NO_2 SCR ($4NH_3 + 3NO_2 \rightarrow 3.5N_2 + 6H_2O$).[6,7]

Zeolite-based catalysts have been proposed as the most promising catalyst formulation for mobile applications, more specifically, iron- or copper-ion-exchanged zeolites.[8] Among zeolite-based materials, MFI, BEA, and CHA frameworks have been successfully used for NH_3-SCR. These types of zeolite frameworks differ in their pore size, i.e., the opening diameters are around 6, 5, and 4 Å for BEA, MFI, and CHA, respectively. In recent years, copper-exchanged SSZ-13 and SAPO-34 zeolites, both with a CHA framework, have been commercially applied in diesel after-treatment systems due to their higher low-temperature activity and hydrothermal stability.[9]

The conventional method to introduce copper into zeolites is liquid ion exchange (LIE). Copper ions (Cu^{2+} or Cu^{+}) can replace cations (NH_4^+, Na^+, H^+, etc.) that are compensating the charge defect introduced by Al atoms replacing Si atoms in the zeolite framework. Thus, the Si/Al ratio governs the ion-exchange capacity of aluminosilicates (e.g., SSZ-13); the more the aluminum content, the more the ability to accommodate Cu ions. However, the previous statement does not apply for aluminosilicophosphates (e.g., SAPO-34) because it depends on where Si is replacing Al or P. In fact, silicon tends to accommodate in the framework forming patches or islands (Si−O−Si),[10] and thus, only silicon ions in the border of the island would create a charge defect to be compensated by cations, limiting the exchange capacity of SAPO-34. Furthermore, the narrow opening diameter of 0.38 nm further impedes the introduction of copper by LIE.

An alternative method to introduce copper ions into zeolites is by solid-state ion exchange (SSIE). The SSIE method relies on heating a physical mixture of the zeolite and a copper

Received: April 18, 2019
Accepted: July 26, 2019
Published: September 5, 2019

DOI: 10.1021/acsomega.9b01118
ACS Omega 2019, 4, 14699−14713

precursor to temperatures near 800 °C.[11,12] This process is reported to be driven by the release of water upon exchange with protons in the zeolite.[13,14] In the present study, SAPO-34 zeolite will be used as zeolite support due to its higher hydrothermal stability with respect to SSZ-13.[15]

The objective of the present paper is to advance the understanding of the formation of different copper species in the SSIE and LIE preparation methods and their roles in NO_x removal from diesel exhaust gases by ammonia selective catalytic reduction (NH_3-SCR). Different Cu species are deeply characterized with scanning electron microscopy (SEM), electronic paramagnetic resonance (EPR), temperature-programmed reduction (H_2-TPR) and desorption (NH_3-TPD), and ultraviolet−visible spectroscopy (UV−vis), specifically focusing on differences between SSIE and LIE preparation methodologies. Furthermore, the comparison of both preparation methodologies is extended to examine the copper loading effect, the nature and location of Cu in the SAPO-34 framework, turnover frequency (TOF) determination, and calculation of activation energies. The superior activity of SSIE with respect to LIE is specifically demonstrated in the present work that, to our knowledge, could not be concluded from papers previously reported in the scientific literature.

2. CONCLUSIONS

Increasing the temperature at which solid-state ion exchange (SSIE) is carried out from 500 up to 700 °C enhances the ability to disperse copper aggregates and promotes the formation of isolated copper ions. In fact, all copper species are detected as aggregates for the sample treated at 500 °C, whereas the proportion of copper ions increases up to 33% in detriment of aggregates for the sample calcined at 700 °C. A further increase in the SSIE temperature negatively affects the stability of the SAPO-34 zeolite framework, leading to some silicon segregation and the loss of specific surface area and acidity. Besides, copper ions tend to agglomerate to form small copper clusters inside the zeolite matrix, and the formation of copper aluminate is favored.

The activation energy of the NH_3-SCR reaction is observed to be in the range of 37−42 kJ mol^{-1}. Only the sample prepared at 500 °C presents a somewhat lower activation energy of 28 kJ mol^{-1}, which suggests some changes in the reaction mechanism ascribed to the absence of copper ions. The Cu/SAPO-34 catalyst prepared at 700 °C by SSIE presents the best NH_3-SCR performance revealed by the highest reaction rate, which was attributed to a higher content of Cu^{2+} ions. However, very similar TOF values are obtained irrespective of the SSIE temperature, which suggests that copper ions are the main active specie for NH_3-SCR.

The SAPO-34 zeolite presents a limited capacity to incorporate copper by liquid ion exchange (LIE). The signal intensity due to Cu^{2+} ions increases linearly up to a copper content of 1.7 wt %, whereas the signal intensity tends to saturate for higher copper loadings, indicating that almost all of the exchangeable locations of the zeolite are already occupied. Thus, copper is preferably incorporated as copper aggregates instead of copper ions for high copper loadings. The presence of residual Na^+ negatively affects the NH_3-SCR performance of catalysts prepared by LIE, whereas a temperature increase during the calcination step up to 700 °C does not significantly change the activity of the sample. On the other hand, SSIE permits the incorporation of copper to a larger extent. However, the signal intensity due to Cu^{2+} ions is maximum for a copper loading of 3.7 wt % and does not further increase with copper loading, revealing again an upper limit to incorporate copper ions by SSIE.

The NH_3-SCR reaction activation energies for samples prepared by LIE and SSIE with different copper loadings are in the ranges of 40−47 and 32−38 kJ mol^{-1}, respectively. Specifically, the sample prepared by LIE with a copper loading of 1.1 wt % presents a lower activation energy, i.e., 19 kJ mol^{-1}, which could be a consequence of a different reaction mechanism due to such a low copper loading. The highest reaction rate values are observed for Cu/SAPO-34 catalysts with low copper loading prepared by either LIE or SSIE due to the preference formation of copper ions instead of aggregates. Very similar TOF values are recorded irrespective of copper loading for catalysts prepared by LIE. Contrarily, a decreasing tendency in TOF is observed for samples prepared by SSIE with increasing copper loading due to a notable penalization of specific surface area. It is observed that TOF values are higher for catalysts prepared by SSIE rather than LIE, which promotes NH_3-SCR.

3. EXPERIMENTAL SECTION

3.1. Catalyst Preparation. Liquid ion exchange (LIE) and solid-state ion exchange (SSIE) were used for preparing Cu/SAPO-34 catalysts. The following procedure was used for LIE. First, H-SAPO-34 powder was contacted with 0.1 M $NaNO_3$ solution to obtain Na/SAPO-34. The ion exchange was conducted for 24 h with continuous stirring at ambient temperature and neutral pH (≈7). The powder was obtained following filtration, washing, and drying overnight at 110 °C. The Na exchange and drying were repeated twice to maximize the exchange ratio, and afterward the sample was calcined at 550 °C for 5 h. Then, Cu/SAPO-34 powder was obtained by ion exchanging Na/SAPO-34 with adequate amounts of $Cu(COOCH_3)_2$ (Panreac, 98%) aqueous solution. This solution (8 g L^{-1}) was stirred for 24 h at 60 °C maintaining the pH value at 6 by ammonia addition (25% as NH_3, Panreac). The suspension was then filtered, washed with deionized water, and dried overnight at 110 °C. Finally, the Cu/SAPO-34 catalyst was obtained by calcining the powder at 500 °C for 4 h.

On the other hand, SSIE Cu/SAPO-34 catalysts were prepared by physically mixing H-SAPO-34 and adequate amounts of CuO nanopowder (Sigma-Aldrich). The precursors were thoroughly mixed until a homogeneous solid was obtained, and afterward calcination was carried out in a reactor placed in a tubular furnace with an airflow of 130 mL min^{-1}. Temperature was elevated from room temperature to the selected maximum temperature (500−800 °C) with a temperature ramp of 1 °C min^{-1}, and temperature was maintained in an isothermal step for 12 h. SSIE Cu/SAPO-34 catalysts were successfully synthesized via this method.

3.2. Catalyst Characterization. *3.2.1. X-ray Fluorescence (XRF).* Wavelength-dispersive XRF analysis was carried out with an AXIOS PANalytical spectrometer equipped with a Rh tube. Prior to the analysis, the sample (200 mg) was mixed with Spectromelt A10 to a solvent/sample weight ratio of 20:1. The melted mixture was poured into a beaker to create a glass disk for analysis.

3.2.2. Surface Area. Textural properties were evaluated from the nitrogen adsorption−desorption isotherms, determined at −196 °C with a Micromeritics TriStar II 3020

DOI: 10.1021/acsomega.9b01118
ACS Omega 2019, 4, 14699−14713

apparatus. The specific surface areas of the samples were determined with the standard Brunauer−Emmett−Teller (BET) procedure, using nitrogen adsorption in the relative equilibrium pressure interval of 0.05−0.2. The samples were previously degassed overnight under nitrogen flow at 300 °C.

3.2.3. X-ray Diffraction (XRD). The XRD patterns of the samples were obtained in a Philips PW1710 diffractometer. The samples were finely ground and were subjected to Cu Kα radiation in the continuous scan mode from 5 to 90° of 2θ with 0.02° s^{-1} sampling interval. PANalytical X'pert HighScore specific software was used for data treatment.

3.2.4. Electronic Paramagnetic Resonance (EPR). EPR spectra were recorded with a Bruker ELEXSYS 500 spectrometer operating at the X-band. The magnetic field was calibrated with an RMN test tube, and the frequency was measured into the cavity with a microwave integrated counter. The temperature was stabilized with an Oxford Instrument regulator (ITC4) at −150 °C. Samples were analyzed in their hydrated form due to exposure to the environment before the analysis.

3.2.5. Temperature-Programmed Reduction (H_2-TPR). Reducibility of Cu in the catalyst was investigated by temperature-programmed reduction (TPR) using H_2 in Micromeritics AutoChem II. The sample (0.25 g) was pretreated in 50 mL min^{-1} of 5% O_2/He gas flow at 450 °C for 60 min and then cooled down. Then, the sample was heated from room temperature to 900 °C with 10 °C min^{-1} ramp in a 50 mL min^{-1} of 5% H_2/Ar mixture gas flow. Water formed during reduction with H_2 was trapped using a cold trap, and hydrogen consumption was continuously monitored with a calibrated thermal conductivity detector (TCD).

3.2.6. Scanning Electron Microscopy (SEM). Copper distribution and the size of copper aggregates were studied using a JEOL JSM-7000F scanning electron microscope equipped with a Schottky field emission gun and an Oxford Inca Pentafet X3 energy-dispersive X-ray (EDX) analyzer. The EDX microanalysis was performed at 20 kV, with a working distance of 10 mm.

3.2.7. Ultraviolet−Visible Spectroscopy (UV−Vis). The oxidation states and the coordination of Cu species were evaluated by diffuse reflectance UV−vis spectroscopy (UV−visible−NIR DRS) with a UV−vis−NIR Cary 5000 apparatus coupled to Diffuse Reflectance Internal 2500 within a range of 200−2500 nm. Prior to the analysis, the samples were dehydrated in air at 350 °C during 3 h.

3.2.8. Temperature-Programmed Desorption of NH_3 (NH_3-TPD). The acidity of the samples was determined in a Micromeritics AutoChem II equipment. The sample (0.08 g) was first pretreated in N_2 with a total flow rate of 50 mL min^{-1} from room temperature to 550 °C with a temperature ramp of 10 °C min^{-1}. Then, 10% NH_3/He was fed at 100 °C until saturation, followed by a purge with 50 mL min^{-1} of He for 1 h to desorb physisorbed NH_3. Finally, the sample was heated from 100 to 550 °C with a temperature ramp of 10 °C min^{-1} in 50 mL min^{-1} of He. The effluent of the reactor was continuously measured by a TCD detector to quantify the NH_3 desorption profile.

3.3. Reactor Experiments. *3.3.1. Selective Catalytic Reduction (NH_3-SCR).* The SCR experiments were performed in a down-flow stainless steel reactor. The reactor tube, with 0.8 g of 0.3−0.5 mm pelletized Cu/SAPO-34 catalyst inside, was located into a three-zone tube furnace. The temperature was measured by a thermocouple at the top of the catalyst bed. The reaction temperature was varied from 150 to 500 °C in steps of 50 °C. The composition of the feed gas mixture was 660 ppm NO, 660 ppm NH_3, and 6% O_2 using Ar as the balance gas. Gases were fed via mass flow controllers, and the total flow rate was set at 2880 mL min^{-1}, which corresponded to a space velocity (gas hourly space velocity) of 86 500 h^{-1}. The NO, NO_2, NH_3, and N_2O concentrations at the reactor exit were monitored every 50 °C, once the analysis had been stabilized for at least 10 min, by an online Fourier transform infrared (FTIR) multigas analyzer (MKS 2030).

The NO (X_{NO}) and NH_3 (X_{NH_3}) conversions were calculated as

$$X_{NO} = \frac{F_{NO}^{in} - F_{NO}^{out}}{F_{NO}^{in}} \times 100 \quad (1)$$

$$X_{NH_3} = \frac{F_{NH_3}^{in} - F_{NH_3}^{out}}{F_{NH_3}^{in}} \times 100 \quad (2)$$

and the N_2, NO_2, and N_2O selectivities, named S_{N_2}, S_{NO_2}, and S_{N_2O}, respectively, were calculated as

$$S_{N_2} = \frac{2F_{N_2}^{out}}{F_{NO}^{in}X_{NO} + F_{NH_3}^{in}X_{NH_3}} \times 100 \quad (3)$$

$$S_{NO_2} = \frac{F_{NO_2}^{out}}{F_{NO}^{in}X_{NO} + F_{NH_3}^{in}X_{NH_3}} \times 100 \quad (4)$$

$$S_{N_2O} = \frac{2F_{N_2O}^{out}}{F_{NO}^{in}X_{NO} + F_{NH_3}^{in}X_{NH_3}} \times 100 \quad (5)$$

where F_i represents the molar flux of "i" species. The superscripts "in" and "out" indicate the molar flow rate being evaluated at the inlet and the exit of the reactor, respectively.

The initial reaction rate approach was employed to determine apparent activation energies. The initial reaction rate was determined with specific experiments carried out under the differential reactor regime, assuring that the NO conversion was below 15% in the whole studied temperature range. The feedstream composition was 660 ppm NO, 660 ppm NH_3, and 6% O_2 using Ar as the balance gas. The NO molar flow at the reactor inlet (F_{NO}) was 2.926×10^{-6} mol s^{-1}, and the catalyst weight (W) was 0.15 g. Previous experiments confirmed that under the experimental conditions, external and internal diffusion resistances are neglected, thus assuring that the observed reaction rate is due to a kinetically controlled regime (Figure S1). Under the differential reactor regime, the initial reaction rate ($-r_{NO}^{o}$, mol NO g^{-1} s^{-1}) can be evaluated by the following expression: $(-r_{NO}^{o}) = X_{NO}/(W/F_{NO}^{o})$, where X_{NO} represents the conversion of NO.[16] The initial reaction rate is normalized per mol of copper (mol NO (mol Cu)$^{-1}$ s^{-1}) dividing the reaction rate by the moles of copper per catalyst gram. Also, the turnover frequency (TOF) can be calculated by dividing the reaction rate normalized per mol of copper by the fraction of copper ions. The representation of the natural logarithm of the initial reaction rate versus the inverse of the reaction temperature allows the evaluation of the apparent activation energy (E_a) from the slope of the linear fitting to the experimental data.

DOI: 10.1021/acsomega.9b01118
ACS Omega 2019, 4, 14699−14713

4. RESULTS AND DISCUSSION

4.1. Influence of Solid-State Ion-Exchange (SSIE) Temperature. For this aim, known amounts of CuO and H-SAPO-34 were mixed and submitted to high temperature, namely, 500, 600, 650, 700, 750, and 800 °C, to favor the solid-state ion exchange. As for reference, a physical mixture of CuO and H-SAPO-34 sample was also prepared without calcination (WO/C). The $Al_2O_3/P_2O_5/SiO_2$ molar composition of the bare H-SAPO-34 was 0.35:0.28:0.15, which was maintained unaltered after the SSIE procedure.

Because some of the SSIE conditions could produce some adverse effect on catalytic behavior of samples, XRD was used to monitor the integrity of the SAPO-34 structure after SSIE. Figure S2 shows X-ray diffraction patterns of prepared catalysts, also including an uncalcined sample and the bare zeolite. The bare zeolite and catalysts prepared at temperatures lower than 700 °C resulted in very similar XRD patterns, which assures that the zeolite structure and crystallinity were maintained unaltered after SSIE. The unique exception with respect to the H-SAPO-34 diffraction pattern is the presence of peaks located at 35.5 and 38.5° 2θ attributed to the presence of copper oxide.[17] This fact suggests that some fraction of copper is probably not ion exchanged and remains as copper aggregates, as any copper ion was not detectable by XRD.[18,19] On the other hand, XRD patterns corresponding to samples calcined at temperatures higher than 700 °C presented an additional phase with a characteristic diffraction peak situated at 21°. This peak, ascribed to silicon dioxide (SiO_2),[13,20] was evident for the Cu/SAPO-34 sample calcined at 750 °C and became the main diffraction peak for the sample treated at 800 °C. Thus, it can be concluded that chemical structure stability of SAPO-34 zeolite was significantly affected only when using temperatures higher than 750 °C, leading to some silicon segregation from the zeolite framework.

Table 1 lists the copper loading and the specific surface area of prepared samples. The elemental composition of samples is reported in Table S1. As can be observed, all catalysts presented very similar copper loadings, around 4.2%. The interaction between copper and zeolite reduces the specific surface area from 600 to 450 $m^2\ g^{-1}$ for samples calcined at temperatures below 700 °C, which is assigned to partial pore blockage by copper aggregates. Further increase in the calcination temperature above 750 °C provokes a decrease in the specific surface area, which resulted in 403 and 270 $m^2\ g^{-1}$ for 750 and 800 °C, respectively. This specific surface area reduction is directly related with a partial destruction of the zeolite framework, as already evidenced by XRD (Figure S2).

Table 1. Copper Loading, BET Surface Area, and Total Acidity of Samples Prepared by SSIE at Different Temperatures

SSIE T, °C	Cu wt %	S_{BET}, $m^2\ g^{-1}$	acidity, μmol $NH_3\ g^{-1}$
SAPO-34		600	1384
500	4.3	452	1449
600	4.3	463	1532
650	4.2	458	1613
700	4.2	447	1571
750	4.2	403	1232
800	4.4	270	853

SEM images were recorded to examine the morphology of SAPO-34 zeolite and determine the size of copper aggregates in the samples prepared under different calcination temperatures. As can be observed in Figure 1, perfect cubic crystals (in light gray) were observed irrespective of calcination temperature, which is in line with the large crystallinity of SAPO-34 detected by XRD. The size of those crystals was rather homogeneous, in the range 2−5 μm, in accordance with previous results in the literature.[13,18,21] Large and numerous copper aggregates (detectable by lighter areas due to the higher atomic number of copper) could be easily observed for the sample calcined at 500 °C (Figure 1a). The number and size of aggregates were progressively reduced while increasing the calcination temperature, as can be observed in Figure 1b for the Cu/SAPO-34 sample calcined at 750 °C. Additional SEM images for the remaining catalysts prepared by SSIE at different temperatures are provided in Figure S3. Thus, it can be concluded that increasing the SSIE calcination temperature enhances the ability to disperse copper aggregates, leading to smaller Cu_xO_y clusters or even copper ions (Cu^{2+}) not detectable by SEM. However, it was evidenced that irrespective of thermal treatment temperature, it was not possible to accomplish complete dispersion of Cu, as copper aggregates located outside the pores of the zeolite were still easily detectable after SSIE.

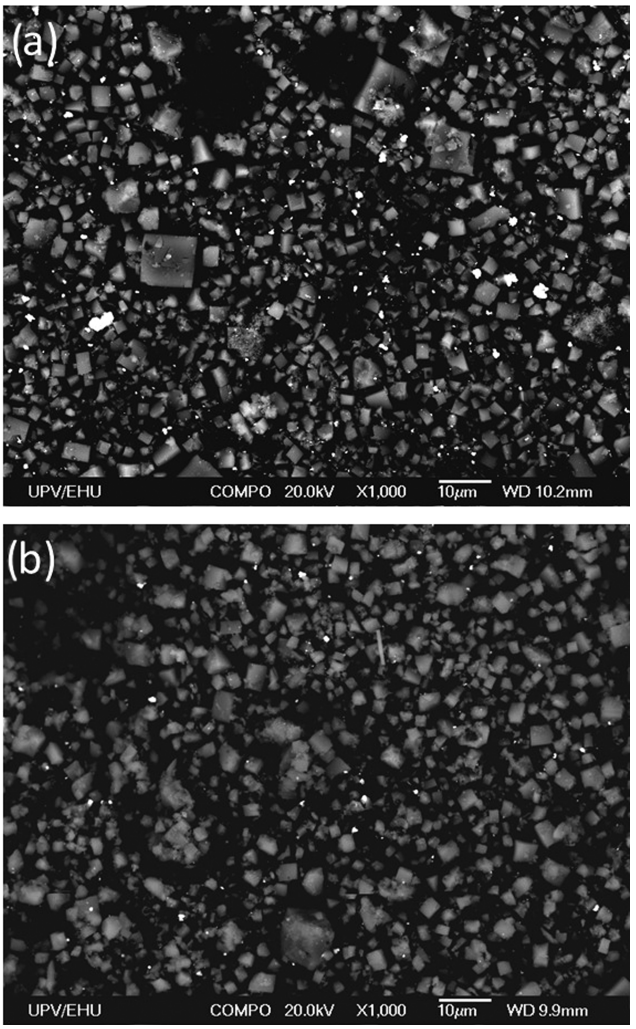

Figure 1. SEM images for the Cu/SAPO-34 catalyst prepared by SSIE at (a) 500 °C and (b) 750 °C.

DOI: 10.1021/acsomega.9b01118
ACS Omega 2019, 4, 14699−14713

Electron paramagnetic resonance (EPR) was used to characterize isolated Cu^{2+} ions,[13,22−24] including aggregated CuO species, and Cu^{+} ions are EPR silent.[25−27] Figure 2 shows

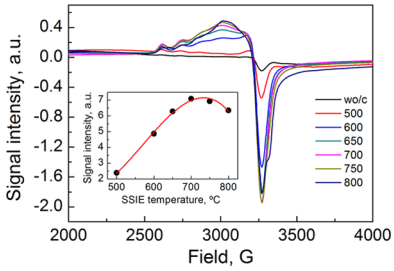

Figure 2. EPR spectra for the Cu/SAPO-34 catalyst prepared by SSIE at different temperatures. The inset of the figure represents the signal intensity calculated by double integral of the original signal in the 2500−3500 field range.

EPR spectra for Cu/SAPO-34 catalysts prepared under different SSIE temperatures, also with a physical mixture of CuO and H-SAPO-34 as reference. All samples presented a characteristic feature at low field (around 1500 G, not shown) attributed to the presence of Fe^{3+} ions.[28,29] The intensity of this signal changed from sample to sample, indicating a nonhomogeneous distribution of Fe^{3+}, which made the quantification of the Cu^{2+} ion content more challenging. Qualitatively, the obtained spectra presented a unique feature in the high-field region at 3270 G, whereas copper hyperfine features are evident at low field. The intensities of low- and high-field features were observed to clearly increase with SSIE temperature. It is worth noting that detection of an additional feature at high field (3315 G) for the sample calcined at 800 °C suggests the presence of two different types of copper ions.

A double integration of the signal presented in Figure 2 in the magnetic field range of 2500−3500 G is shown in the inside figure, which allows a semiquantitative comparison among the prepared samples. As can be observed, signal intensity due to the presence of isolated Cu^{2+} ions increases monotonically with SSIE temperature up to 700 °C. Afterward, the signal intensity tends to be saturated or even decrease, which suggests that further increase of temperature above 700 °C did not result in the formation of higher amount of copper ions. By analyzing the hyperfine features, $g_{\parallel}$ = 2.39 and $A_{\parallel}$ = 132 G are obtained, which is consistent with an octahedral coordination of Cu^{2+} ions.

Figure 3 shows H_2 consumption profiles from temperature-programmed reduction (H_2-TPR) experiments for Cu/SAPO-34 catalysts prepared by SSIE under different calcination temperatures. Generally, the reduction of Cu^{2+} ions in zeolites takes place through two consecutive steps, i.e., Cu^{2+} ions reduce to Cu^{+} and subsequent reduction of Cu^{+} ions to Cu^{0}.[16,25,30,31] Moreover, it has been reported that reduction of CuO nanoparticles to Cu^{0} occurs in a single step at around 300 °C.[16,32] However, in accordance with results reported by Wang et al.,[33] we determined experimentally that a physical mixture of CuO and SAPO-34 zeolite presented a single reduction peak located at a lower temperature, ca. 260 °C (bottom left graphic in Figure 3), undoubtedly assigned to reduction of CuO aggregates to Cu^{0}.

The SSIE procedure at 500 °C did not modify the redox behavior of the sample with respect to the physical mixture CuO/SAPO-34. However, some changes started becoming

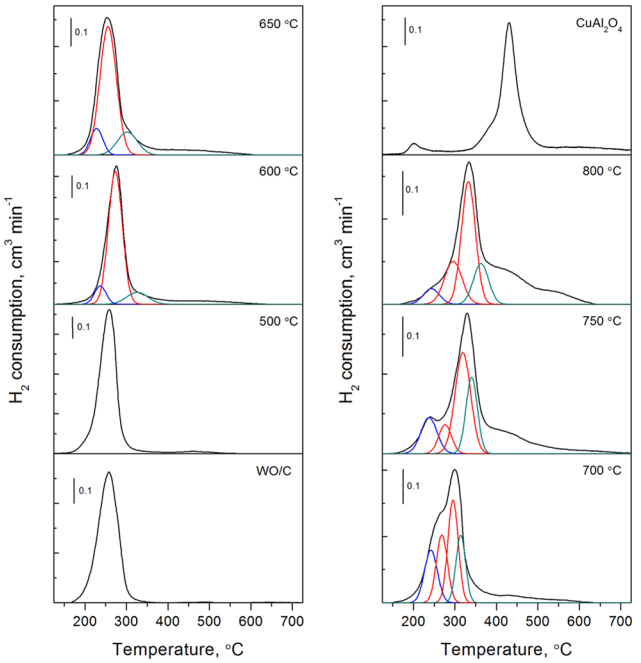

Figure 3. H_2 consumption profiles during H_2-TPR experiments for the Cu/SAPO-34 catalyst prepared by SSIE at different temperatures. Experiments with a physical mixture of CuO and SAPO-34 without being calcined (WO/C) and copper aluminate are also included as a reference.

evident for the sample submitted to SSIE at 600 °C, i.e., a small H_2 consumption peak centered around 320 °C started to develop. Reduction of Cu^{2+} ions to Cu^{+} has been reported to occur at temperatures lower than 250 °C,[16,25,34] whereas subsequent reduction of Cu^{+} ions to Cu^{0} occurs at higher temperatures. Thus, we are considering that reduction of Cu^{2+} ions to Cu^{+} occurs around 230 °C, reduction of large copper aggregates occurs around 260 °C, and final reduction of Cu^{+} ions occurs at 320 °C. Note that coexistence of copper ions (Cu^{2+}) and CuO aggregates has been already evidenced by EPR and SEM, respectively, in the prepared samples.

It was not straightforward to determine the size and amplitude of the low-temperature H_2 consumption contribution due to reduction of Cu^{2+} to Cu^{+} ions. However, the observed H_2/Cu ratio for the whole H_2-TPR experiment (Table 2) is very close to 1 in all cases, which indicates that all copper exist in an oxidation state +2 in the original sample; thus, the area of the low-temperature contribution ($Cu^{2+} \rightarrow Cu^{+}$) located at 230 °C should be very close to the area of the high-temperature contribution ($Cu^{+} \rightarrow Cu^{0}$) located at 320 °C.

Samples treated at temperatures higher than 700 °C required an additional contribution to adequately describe the observed H_2 consumption profile. In particular, this contribution was located at 300 °C and was assigned to the reduction of nanosized copper clusters (Cu_xO_y),[16] which interact more strongly with the support and consequently require higher temperatures than that needed for large copper aggregates (260 °C) to be reduced. This observation is in agreement with results previously reported by Gao et al.[13] who attributed the temperature shift of the major reduction peak to higher temperatures associated with changes in dispersion of the CuO nanoparticles.

DOI: 10.1021/acsomega.9b01118
ACS Omega 2019, 4, 14699−14713

Table 2. Quantification of H_2 Consumption Attributed to the Reduction of Different Copper Species along with Copper Species Distribution and H_2/Cu Ratio

	H_2 consumption due to, μmol g^{-1}						Cu species distribution, %				
sample	$Cu^{2+} \rightarrow Cu^{+}$	$CuO \rightarrow Cu^0$, aggregates	$CuO \rightarrow Cu^0$, clusters	$Cu^{+} \rightarrow Cu^0$	$CuAl_2O_4$	Cu^{2+}	CuO aggregates	CuO clusters	Cu^{+}	$CuAl_2O_4$	H_2/Cu
WO/C		538.3					100				0.93
500 °C		643.1					100				0.94
600 °C	61.8	472.0		75.8	78.6	18	67		4	11	0.99
650 °C	83.2	382.5		93.9	88.5	25	58		3	13	1
700 °C	107.2	136.0	175.1	113.9	106.4	33	21	27	2	16	0.91
750 °C	89.2	50.4	244.6	101.7	150.6	27	8	38	4	23	0.93
800 °C	56.4	59.9	269.4	75.7	177.9	17	9	41	6	29	0.85

Finally, samples treated at temperatures higher than 600 °C presented an additional H_2 consumption contribution centered around 450 °C with a long tail up to 650 °C. This contribution was assigned to the reduction of highly stable copper ions in the copper aluminate ($CuAl_2O_4$) phase, whose formation has already been reported for copper zeolites under specific preparation conditions.[13,35] To verify this assignation, bulk $CuAl_2O_4$ was synthesized by mixing nanopowder CuO and γ-Al_2O_3 and calcining the physical mixture at 1000 °C. The H_2-TPR experiment included in Figure 3 (top right graphic) revealed a main hydrogen consumption peak at 430 °C for $CuAl_2O_4$, which validates the previous assignation. It is worth noting that the presence of $CuAl_2O_4$ begins to be significant for temperatures higher than 750 °C, in line with detection of some segregated silicon oxide from the zeolite framework by XRD. Thus, it seems that such a high temperature is able to produce a partial destruction of the zeolite framework, leading to some recombination of atoms to form SiO_2 and $CuAl_2O_4$ along with the original SAPO-34. Furthermore, formation of $CuAl_2O_4$ can also be well correlated with detection of two different types of Cu^{2+} ions by EPR for samples treated at 750 and 800 °C.

Integration of H_2 consumption peaks observed in Figure 3 with time permitted us to calculate the amount of hydrogen (μmol H_2 g^{-1}) consumed during reduction of copper ions in sequential steps, reduction of copper aggregates and copper clusters, and reduction of copper aluminate, following a similar trend to that reported elsewhere.[36−39] Furthermore, it was possible to determine the relative abundance of different types of copper species in the original sample (Table 2) based on reduction stoichiometry. For example, the sample treated at 700 °C presented a hydrogen consumption of 107.2 μmol H_2 g^{-1} for reduction of Cu^{2+} ions to Cu^{+} ions, which means that 214.4 μmol Cu^{2+} g^{-1} was present in the original sample based on its reduction stoichiometry: $Cu^{2+} + 1/2H_2 \rightarrow Cu^{+} + H^{+}$. Then, 136.0 and 175.1 μmol H_2 g^{-1} were used for reduction of copper aggregates and copper clusters, respectively, both following the same reduction stoichiometry: $CuO + H_2 \rightarrow Cu^0 + H_2O$, which results in contents of copper aggregates and clusters of 136.0 and 175.1 μmol g^{-1}, respectively. The amount of hydrogen used for reduction of Cu^{+} ions to metallic copper was 113.9 μmol H_2 g^{-1}. However, calculation of the amount of Cu^{+} ions in the original sample requires subtraction of hydrogen consumption due to reduction of Cu^{+} ions coming from Cu^{2+} ion reduction. Thus, hydrogen consumption attributed to Cu^{+} ion reduction can be calculated by 113.9−107.2 μmol H_2 = 6.7 μmol H_2 g^{-1}, and taking into account the reduction stoichiometry ($Cu^{+} + 1/2H_2 \rightarrow Cu^0 + H^{+}$), the content of Cu^{+} ions results in 13.3 μmol g^{-1}. Finally, hydrogen consumption due to reduction of copper aluminate was 106.4 μmol H_2 g^{-1}, and consequently the amount of copper aluminate was 106.4 μmol g^{-1} based on its reduction stoichiometry ($CuAl_2O_4 + H_2 \rightarrow Cu^0 + Al_2O_3 + H_2O$).

The proportions of different types of copper species are tabulated in Table 2. As can be observed, SSIE carried out at 500 °C is not able to produce any change with respect to the noncalcined sample, and all copper remained as aggregates. Further increase in the calcination temperature up to 600 °C results in the formation of copper ions in detriment of large aggregates. The proportion of Cu^{2+} ions increased progressively with SSIE temperature, reaching a maximum value of 33% at 700 °C, in line with EPR results, whereas the proportion of CuO aggregates is complementarily reduced. Small copper clusters begin to become detectable for SSIE temperatures of 700 °C and onward. A further temperature increase up to 800 °C penalized formation of copper ions probably due to agglomeration of copper ions to form small copper clusters inside the zeolite framework. The proportion of Cu^{+} ions was below 6% for all prepared samples, in line with experimentally detected H_2/Cu ∼ 1 as experimentally determined. Finally, copper aluminate started to become detectable at calcination temperature of 600 °C with progressive promotion of its formation with temperature, reaching a maximum value of 29% at 800 °C. To sum up, it can be concluded that progressive increase in the temperature at which SSIE is carried out favors the formation of copper ions up to 700 °C, whereas further temperature increase promotes the formation of small copper clusters and copper aluminate.

Table 1 also includes the total acidity of samples determined by NH_3-TPD. As can be observed, the total acidity of samples increased progressively with SSIE temperature up to 650 °C. This fact is ascribed to the formation of Cu^{2+} ions, providing the catalyst with a higher amount of Lewis acid sites that promotes NH_3 storage.[21,27,33,40] However, total acidity of samples tends to decrease when SSIE was carried out at temperatures higher than 650 °C. Note that total acidity of the sample prepared by SSIE at 800 °C was even lower than that observed for the bare zeolite. We suggest, in accordance with XRD results, that such a high temperature is able to produce a partial destruction of the zeolite framework (evidenced by SiO_2 segregation), which ultimately reduces the population of Brönsted acid sites and leads to a lower NH_3 adsorption capacity. Besides, the formation of copper clusters, in detriment to copper ions, while increasing the SSIE temperature above 700 °C also reduces the availability of Lewis acid sites to store NH_3.

UV−vis DRS spectra were determined to complete the analysis of copper species in the prepared samples by SSIE.[22,27]

DOI: 10.1021/acsomega.9b01118
ACS Omega 2019, 4, 14699−14713

The overall spectra (Figure S4) are similar to those reported for Cu-zeolites such as Cu/SSZ-13,[11] as well as Cu/SAPO-34.[21,41,42] Two main characteristic absorption bands were observed for all of the samples. The one centered at ca. 240 nm is attributed to a charge transfer band of the zeolite,[21,43] and a broad band in the region of 300−800 nm was attributed to the presence of CuO,[11] as evidenced by the UV−vis spectra of a physical mixture of CuO and H-SAPO-34 and also the bulk CuO sample. This broad band is composed of several bands at ca. 355 and 456 nm assigned to the charge transfer bands of O−Cu−O and Cu−O−Cu complexes, respectively,[44,45] and a broad absorption band at 600−800 nm assigned to the electron d−d transitions of Cu^{2+} in distorted octahedral coordination surrounded by oxygen in dispersed CuO particles.[21,45] As can be observed, the physical mixture of CuO and H-SAPO-34 presents a broad absorption band in the Ultraviolet−visible and near-infrared region, i.e., 300−800 nm. The absorption intensity was progressively reduced on increasing the SSIE temperature until it became minimum for treating temperatures of 700 °C, revealing that the population of aggregated CuO species was progressively reduced. Finally, SSIE temperatures of 750 and 800 °C presented a higher absorption intensity around 350−600 nm, assigned to the presence of copper aluminate.[11]

Figure 4 illustrates NO and NH_3 conversions and selectivity toward N_2, N_2O, and NO_2 as a function of the reaction

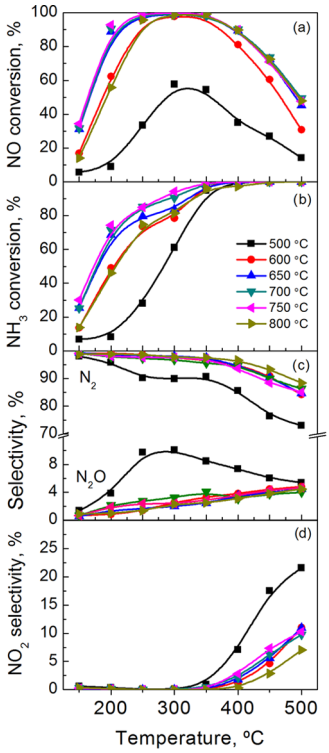

Figure 4. Evaluation of NH_3-SCR performance for samples prepared by SSIE at different temperatures: (a) NO conversion, (b) NH_3 conversion, (c) N_2 and N_2O selectivities, and (d) NO_2 selectivity.

temperature during NH_3-SCR experiments with the Cu/SAPO-34 catalyst prepared by SSIE at different temperatures. As can be observed, the catalyst prepared at 500 °C presents very limited NH_3-SCR performance, reaching a maximum NO conversion of 58% at 300 °C (Figure 4a). Increasing temperature at which SSIE is performed results in a noteworthy enhancement of NO conversion. In fact, the Cu/SAPO-34 catalyst prepared at 600 °C obtained maximum NO conversion of 98% at 300 °C. NH_3-SCR activity enhancement can be related to formation of copper ions in detriment of large aggregates, and, thus, points out that these copper ions are more active than aggregates. Further increase in the SSIE temperature up to 750 °C results in a broadening of the NO conversion performance, increasing low- and high-temperature NH_3-SCR activity. Although the contents of large copper aggregates and small copper clusters changed markedly among samples calcined at 650, 700, and 750 °C, they presented almost identical NH_3-SCR activity due to comparable amounts of copper ions, situated in the range of 26−33% (Table 2). Further temperature increase up to 800 °C favored the migration of copper ions into the partially destroyed zeolite matrix to form $CuAl_2O_4$, which reduces the availability of copper species at the surface to activate the NH_3-SCR reaction and consequently presents a lower NH_3-SCR activity specifically at low temperatures. Furthermore, the lower catalytic activity of the sample calcined at 800 °C could be also correlated with the lower specific surface area and lower acidity (Table 1).

NH_3 conversion (Figure 4b) follows a similar trend to that observed for NO, but specifically it can be observed that the sample prepared at 750 °C presents the highest NH_3 conversion in the whole studied temperature range. At high temperature, the NH_3 oxidation reaction starts to prevail and thus total NH_3 conversion is obtained for temperatures of 400 °C and onward for all prepared catalysts.[8,46] Reaction between NH_3 and oxygen reduces the availability of the reductant and consequently NO conversion starts to decrease for temperatures higher than 400 °C, as already observed in Figure 4a.

Figure 4c shows the selectivity toward N_2 and N_2O, whereas Figure 4d presents the selectivity toward NO_2 in the studied temperature range. As can be observed, all prepared samples presented high selectivity to nitrogen and reduced selectivity to N_2O. Selectivities to N_2 and N_2O are complementary up to 350 °C; formation of NO_2 becomes significant only at higher temperatures due to the NO-to-NO_2 oxidation reaction. Focusing on N_2O selectivity, a progressive increase with temperature can be observed, although it is always maintained below 5%. Specifically, the sample prepared at 500 °C presented higher N_2O selectivity, showing a maximum of 10% around 300 °C, which is related to the decomposition of ammonium nitrate.[47,48] Besides, this sample also presented a notable higher NO_2 selectivity, reaching 22% at 500 °C. Thus, it can be suggested that copper species have a notable impact on the NH_3-SCR product distribution. Large copper aggregates favor the formation of N_2O and enhance the oxidation capacity of the sample, promoting selectivity to NO_2. On the other hand, copper ions, even if they are in a minor relative abundance with respect to aggregates or clusters, are able to drive the NH_3-SCR reaction selectively toward nitrogen.

To better discern the NH_3-SCR activity of the prepared samples, additional reaction experiments were carried out under a differential reactor regime assuring that NO conversion was maintained below 15% in the whole studied temperature range for easy calculation of the initial reaction rate, activation energy, and turnover frequency (TOF); these values are listed in Table S3. Figure 5 shows the Arrhenius plot to calculate apparent activation energies. As can be observed, irrespective of the temperature at which SSIE was carried out,

DOI: 10.1021/acsomega.9b01118
ACS Omega 2019, 4, 14699−14713

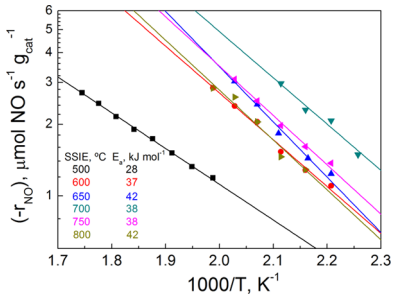

Figure 5. Arrhenius plot for the determination of the activation energy for samples prepared by SSIE at different temperatures. (Note the logarithmic scale in the *Y* axis.)

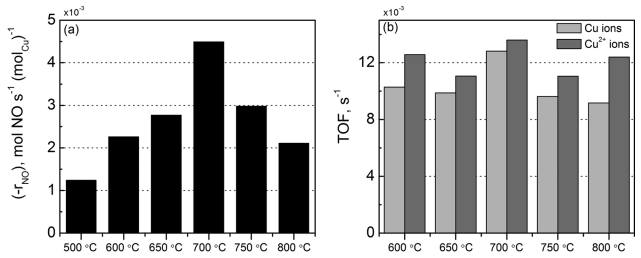

Figure 6. Evolution of the reaction rate (a) and the turnover frequency (b) as a function of SSIE temperature. TOF values are referred to the total amount of copper ions or alternatively to the amount of Cu^{2+} ions quantified by H_2-TPR.

the apparent activation energy was around 40 kJ mol^{-1}, which means that the NH_3-SCR reaction proceeds through the same reaction mechanism. The observed activation energy is very close to that reported by Hu et al.[49] with Cu/SAPO-34 catalysts prepared by one-pot synthesis and different crystal sizes of zeolite, i.e., 44.8 kJ mol^{-1}. Besides, Hu et al. provided different activation energies from other works[16,21,25,33,50,51] using Cu/SAPO-34 catalysts at different reaction temperatures (100−225 °C) and copper loadings (0.35−6.78 wt %), revealing that all were situated between 34 and 45 kJ mol^{-1}. Specifically, the sample prepared by SSIE at 500 °C presented a lower activation energy of 28 kJ mol^{-1}. Specific experiments were carried out with this sample verifying the absence of internal diffusion limitations (Figure S1). Changes in the activation energy at low temperatures (<250 °C) were also reported by Gao et al.,[23] who justified this observation by assuming that different types of active centers or locations were affecting the kinetic analysis. In this sense, we can speculate that the different activation energy observed for the sample prepared by SSIE at 500 °C is due to the presence of large copper aggregates as the main active center, although the presence of small quantities of copper ions cannot be totally ruled out due to migration of copper species under standard SCR conditions.[12,52,53] On the other hand, all remaining samples presented a noticeable portion of copper ions, which led to the same activation energy.

More specifically, the reaction rate normalized per mol of copper, $-r_{NO}$ (mol NO (mol Cu)$^{-1}$ s^{-1}), and the turnover frequency, TOF (s^{-1}), were calculated. TOF values have been normalized to the total amount of Cu^{2+} ions,[24,49] as those species have been considered the active site for NH_3-SCR.[50,54,55] Additionally, we have also included the calculation of TOF based on the total amount of copper ions (Cu^{2+} and Cu^{+}). On the other hand, the reaction rate normalized per mol of copper ($-r_{NO}$) has also been used to compare the NH_3-SCR activity of different catalysts.[21,56,57] In the present study, we have calculated the reaction rate normalized per mol of copper, ($-r_{NO}$), by dividing the reaction rate by the moles of Cu per gram of catalyst. TOF has been calculated by dividing the reaction rate normalized per mol of copper by the fraction of Cu^{2+} ions or by the fraction of total copper ions (Cu^{2+} and Cu^{+}) quantitatively determined by H_2-TPR (Table 2).

Figure 6a shows the evolution of the reaction rate normalized per mol of copper at 200 °C for catalysts prepared by SSIE at different temperatures. As can be observed, the evolution of ($-r_{NO}$) with SSIE temperature presents a maximum at 700 °C (4.5×10^{-3} mol NO (mol Cu)$^{-1}$ s^{-1}). The reaction rate profile correlates very well to the proportion of copper ions, which was maximum (33%) for the sample prepared at 700 °C. Thus, it can be deduced that Cu^{2+} ions are the main active species for NH_3-SCR, although large copper aggregates also present some activity based on the reaction rate calculated for the sample calcined at 500 °C (1.2×10^{-3} mol NO (mol Cu)$^{-1}$ s^{-1}). At this point, it is worth noting that recent papers[12,52,53,58−61] have suggested the mobility of copper species under NH_3-SCR conditions, and thus, the speciation of copper may shift during activity measurements. Figure 6b shows the evolution of TOF referred to the content of Cu^{2+} ions or the total content of Cu ions for the prepared samples except for that calcined at 500 °C, in which copper ions are absent. As can be observed, similar TOF values, around 12×10^{-3} s^{-1}, are observed irrespective of calcination temperature, which suggests the presence of similar copper ions with the same NH_3-SCR activity, as already reported elsewhere.[16] A similar trend is observed when TOF is referred to the total amount of copper ions.

4.2. Influence of Copper Loading in Cu/SAPO-34 Samples Prepared by Liquid Ion Exchange (LIE) and Solid-State Ion Exchange (SSIE). Four Cu/SAPO-34 catalysts were prepared by liquid ion exchange (LIE) and subsequent calcination at 500 °C. Different copper concentrations were used in the starting solution to achieve increasing copper loading in the prepared samples. On the other hand, five Cu/SAPO-34 catalysts were prepared by SSIE at the optimum temperature as deduced in the previous section, i.e., 700 °C, with nominal copper loadings of 2, 4, 6, 8, and 10 wt %.

Table 3 lists the copper loading, BET surface area, and acidity of the prepared samples by SSIE and LIE. The complete elemental composition of samples is reported in Table S2. As can be observed, BET surface area slightly decreases after the LIE procedure with respect to bare zeolite (600 m^2 g^{-1}). However, Cu loading does not have a great impact on surface area, which remains around 489−517 m^2 g^{-1}, with a slight tendency to decrease with increasing Cu loading due to the preferential formation of some copper aggregates. When comparing LIE and SSIE samples with similar Cu content, it can be observed that the specific surface area is notably higher for samples prepared by LIE. Specifically, the sample prepared by LIE with a copper loading of 3.6% presented a specific surface area of 489 m^2 g^{-1}, which is notably higher than that presented by the sample prepared by SSIE with a copper loading of 3.7%, 397 m^2 g^{-1}. Note that specific surface area critically decreases for copper loadings higher than 6% for samples prepared by SSIE due to pore blockage by copper aggregates. In fact, the specific surface area

DOI: 10.1021/acsomega.9b01118
ACS Omega 2019, 4, 14699−14713

Table 3. Copper Loading, BET Surface Area, and Total Acidity of Samples Prepared by LIE and SSIE

preparation method	nominal Cu loading, %	Cu wt %	surface area, $m^2\ g^{-1}$	acidity, μmol $NH_3\ g^{-1}$
H-SAPO-34			600	1384
LIE	1	1.1	504	1112
	2	1.7	517	1652
	4	2.2	509	1247
	10	3.6	489	1540
SSIE	2	1.9	483	1402
	4	3.7	397	1348
	6	5.8	322	1533
	8	7.9	190	990
	10	9.8	44	399

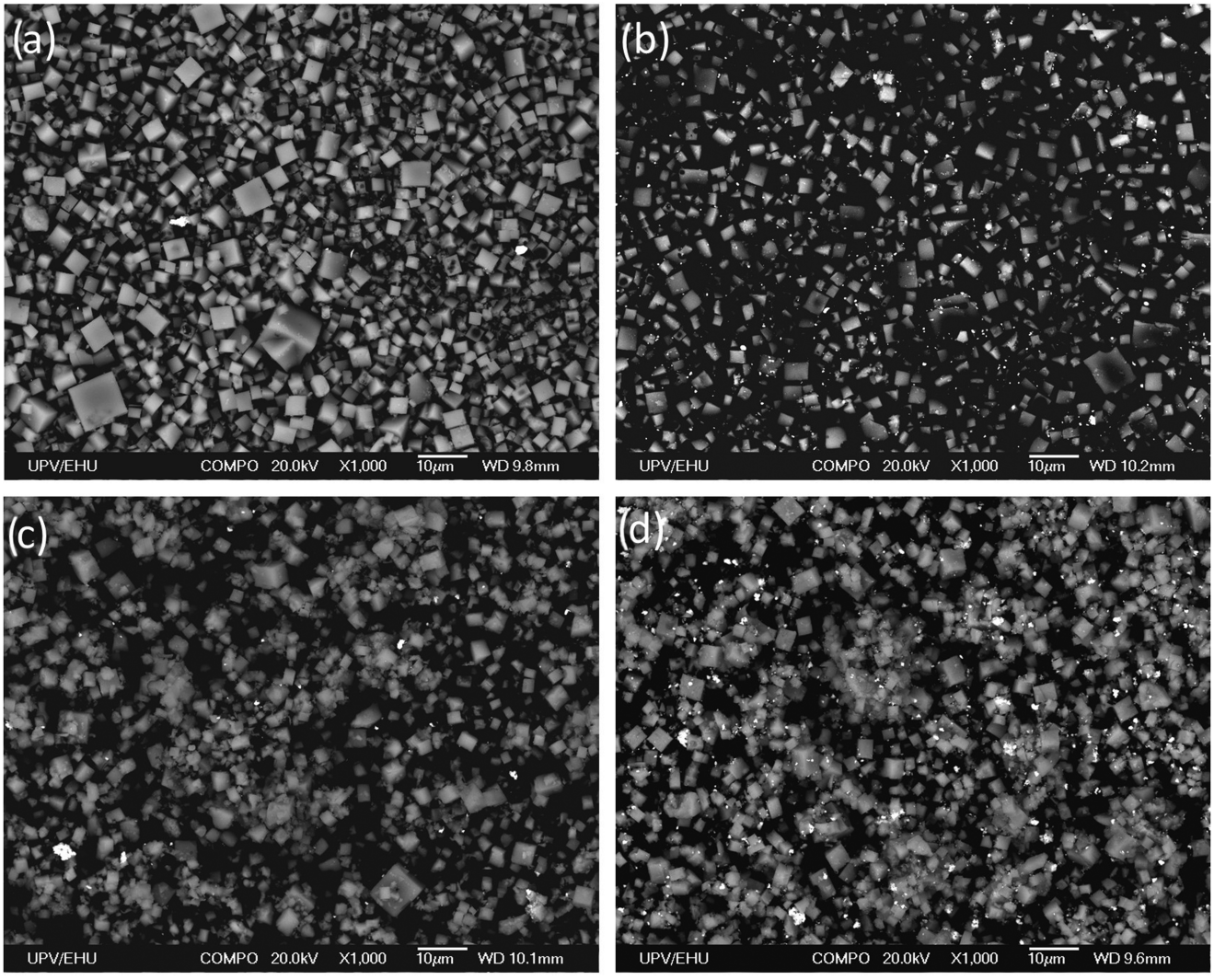

Figure 7. SEM images for the Cu/SAPO-34 catalyst prepared by LIE with copper loadings of 1.7% (a) and 3.6% (b) and SSIE with copper loadings of 1.9% (c) and 9.8% (d).

of the sample with a nominal copper loading of 10% decreases to 44 $m^2\ g^{-1}$.

Figure S5 shows XRD diffraction patterns of prepared LIE and SSIE samples. XRD patterns confirmed that the SAPO-34 framework was maintained unaltered after LIE, without significant crystallinity loss, irrespective of Cu loading. Furthermore, CuO characteristic diffraction peaks, located at 35.5 and 38.5° 2θ, were not detected even for a high copper-loaded catalyst, suggesting that isolated copper ions or highly dispersed Cu_xO_y clusters, both beyond the XRD detection limit,[18,19] are predominant copper species in samples prepared by LIE. On the other hand, all catalysts prepared by SSIE presented diffraction peaks attributed to CuO with increasing intensity as increasing copper loading. Besides, all catalysts also presented some SiO_2 segregation detected at 21°. The intensity of that diffraction peak increased notably with copper loading, revealing that high copper loading favors collapse of the zeolite structure, which can also be evidenced by the

DOI: 10.1021/acsomega.9b01118
ACS Omega 2019, 4, 14699−14713

almost total disappearance of the main diffraction peak of SAPO-34 situated at 10°.

Figure 7 shows SEM images of catalysts prepared by LIE and SSIE. On the one hand, it was difficult to find copper aggregates by SEM in low copper-loaded samples prepared by LIE. In particular, only two large CuO aggregates with a particle size around 1 μm were observed for the 1.7% Cu/SAPO-34 catalyst (Figure 7a). The picture changed radically for the 3.6% Cu/SAPO-34 catalyst, where a very large number of CuO particles were easily distinguishable (Figure 7b). On the other hand, numerous large copper particles were evident even for the low copper-loaded catalyst prepared by SSIE (1.9% Cu/SAPO-34, Figure 7c), and the number of those aggregates further increased with copper loading (9.8% Cu/SAPO-34, Figure 7d). From Figure 7, it can be also inferred that SSIE reduces crystallinity of the zeolite (as already observed by XRD), as the perfect cubic crystals observed for catalysts prepared by LIE tend to become highly irregular after the temperature treatment during SSIE.

EPR spectra for samples prepared by LIE and SSIE are displayed in Figure 8a,b, respectively. The catalyst prepared by

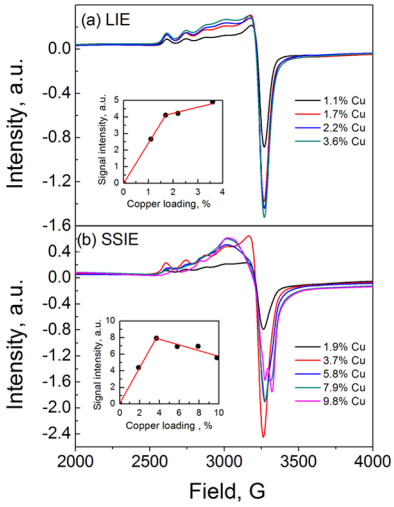

Figure 8. EPR spectra for the Cu/SAPO-34 catalyst prepared by LIE and SSIE with varying copper loadings. The insets of the figures represent the signal intensity calculated by the double integral of the original signal in the 2500−3500 field range.

LIE presented a unique feature at high field and well-resolved copper hyperfine features at low fields. On the contrary, samples prepared by SSIE presented an additional feature at high field (3323 G) for samples with a copper loading above 6%, whose intensity increases with copper loading and can be related to the presence of copper aluminate. The copper ion signal intensity calculated by a double integral can be observed in the inset of each figure. As can be observed, Cu^{2+} signal intensity increases linearly for samples prepared by LIE up to a copper loading of 1.7 wt %, whereas for higher copper loadings, the signal intensity tends to saturate, indicating that almost all exchangeable locations of the zeolite have already been occupied and only a few more copper ions can be included by LIE. A similar trend was observed for samples prepared by SSIE, but instead the signal intensity increased linearly up to a copper loading of 3.7 wt %. A higher copper loading did not result in a signal intensity increase, which also reveals an upper limit to incorporate copper ions by SSIE.

Figure 9 shows H_2 consumption profiles during temperature-programmed reduction (H_2-TPR) experiments for Cu/

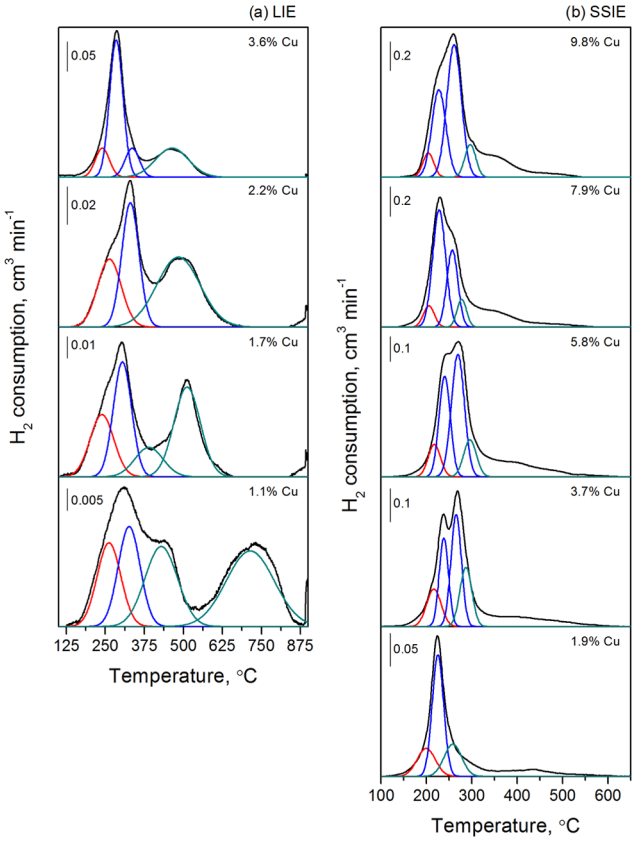

Figure 9. H_2 consumption profiles during H_2-TPR experiments for the Cu/SAPO-34 catalyst prepared by LIE and SSIE with different copper loadings.

SAPO-34 catalysts prepared by LIE and SSIE with different copper loadings. Focusing on samples prepared by LIE and following the previous assignation, the low-temperature peak (240 °C) was ascribed to the reduction of Cu^{2+} ions to Cu^{+}. At higher temperatures (300 °C), reduction of small copper clusters to metallic copper occurred in a single step (CuO → Cu^0), and for high copper loading samples, an additional hydrogen consumption was observed at somewhat lower temperatures (280 °C) due to reduction of large copper aggregates. The final reduction of Cu^{+} ions to Cu^0 was affected by copper loading. The Cu/SAPO-34 catalyst with copper loadings higher than 1.7% presented a single reduction contribution around 480 °C. On the other hand, two contributions were needed to describe Cu^{+} → Cu^0 reduction in low copper-loaded SAPO-34 catalysts; furthermore, Cu^{+} ion reduction required higher temperatures. In fact, highly stable Cu^{+} ion (namely, H-Cu^{+}) reduction occurred at temperatures as high as 790 °C for the 1.1% Cu/SAPO-34 catalyst, which has already been reported in the literature.[62,63] Torre-Abreu et al.[31] have also reported the ease of Cu^{+} ion reduction with increasing copper loading.

Table 4 shows hydrogen consumption quantification for each reduction step, i.e., Cu^{2+} → Cu^{+}, CuO → Cu^0, and Cu^{+} → Cu^0, and the proportion of copper species based on previous H_2 consumption and reduction stoichiometry. Isolated Cu^{2+} and Cu^{+} ions were predominant in low copper loading samples, whereas the proportion of CuO clusters

DOI: 10.1021/acsomega.9b01118
ACS Omega 2019, 4, 14699−14713

Table 4. Quantification of H_2 Consumption Attributed to the Reduction of Different Copper Species along with Copper Species Distribution and H_2/Cu Ratio

LIE catalysts	H_2 consumption due to, μmol g^{-1}			Cu species distribution, %			H_2/Cu
Cu wt %	$Cu^{2+} \rightarrow Cu^{+}$	$CuO \rightarrow Cu^0$	$Cu^{+} \rightarrow Cu^0$	Cu^{2+}	CuO	Cu^{+}	experimental
1.1	21.3	25.5	64.2	28	17	56	0.57
1.7	61.1	84.5	136.1	34	24	42	0.87
2.2	63.2	90.4	125.3	37	27	36	0.83
3.6	58.9	292.3	133.8	21	52	27	0.87

SSIE catalysts	H_2 consumption due to, μmol g^{-1}					Cu species distribution, %					H_2/Cu
Cu wt %	$Cu^{2+} \rightarrow Cu^{+}$	$CuO \rightarrow Cu^0$ aggregates	$CuO \rightarrow Cu^0$ clusters	$Cu^{+} \rightarrow Cu^0$	$CuAl_2O_4$	Cu^{2+}	CuO aggregates	CuO clusters	Cu^{+}	$CuAl_2O_4$	experimental
1.9	40.3	115.4		46.3	38.8	33	47		5	16	0.80
3.7	78.5	133.9	176.2	109.5	88.3	25	22	29	10	14	0.93
5.8	84.3	299.7	264.4	90.1	173.5	18	33	29	1	19	0.87
7.9	89.9	492.9	376.7	116.0	182.8	14	38	29	4	14	0.89
9.8	92.1	430.3	512.1	120.4	290.2	13	29	35	4	20	0.90

progressively increased at the expense of copper ions while the copper content was increased. This fact reveals a limited quantity of exchangeable sites in SAPO-34 zeolite to accommodate copper ions, in line with EPR results.

Figure 9 also includes H_2-TPR experiments for Cu/SAPO-34 samples prepared by SSIE with different copper loadings. The H_2 consumption contributions have been assigned, as in the previous section with SSIE catalysts calcined at different temperatures, to reduction of Cu^{2+} ions to Cu^{+}, reduction of large CuO aggregates to Cu^0, reduction of small CuO clusters to Cu^0, and reduction of Cu^{+} ions to Cu^0 with increasing reduction temperature. Figure 9 allows a proper comparison between hydrogen reduction profiles of samples prepared by LIE and SSIE. The main difference between both preparation methods is that reduction of Cu^{2+} and more notably reduction of Cu^{+} ions occurred at lower temperatures for samples prepared by SSIE. We suggest that the LIE preparation methodology incorporates more specifically copper ions at exchangeable sites with a higher interaction with the support, e.g., at 6dr windows of the CHA structure, which hinders their reduction. On the other hand, copper ions introduced by the SSIE preparation methodology could be located at CHA cages with lower interaction with the support, which facilitates their reduction. Besides, formation of copper dimers during SSIE could also be responsible for shifting the reduction profile to lower temperatures.[64] Table 4 also includes the copper species distribution for samples prepared by SSIE. As can be observed, the low copper content sample presents the highest proportion of copper ions, although small copper clusters are the predominant species. With increasing copper loading, the proportion of copper ions decreased in favor of copper aggregates and clusters. Finally, the proportion of $CuAl_2O_4$ is similar because the same calcination protocol was used for all prepared samples and, as deduced from the previous section, copper aluminate formation is only promoted by the temperature at which the SSIE procedure took place. In this sense, copper aluminate is not detected in samples prepared by LIE due to the lower calcination temperature, i.e., 500 °C.

The NH_3-SCR activity of samples prepared by LIE and SSIE with different copper loadings has been provided in Figure 10. A clear promotion of low-temperature NH_3-SCR activity can be observed for the LIE catalyst on increasing the copper loading from 1.1 to 2.2%, as already reported in a previous work[64] for β and ZSM-5 zeolites. The promotion of low-temperature NH_3-SCR activity for the SSIE catalyst on increasing the copper loading was not so evident, and only a slight promotion of NO conversion was observed from 1.9 to 3.7% of Cu. It is worth noting that the SSIE preparation methodology resulted in a more active Cu/SAPO-34 catalyst for low-temperature NH_3-SCR in comparison to those prepared by LIE. For example, at 200 °C, NO conversion was 41% for the 1.7% Cu/SAPO-34 catalyst prepared by LIE, whereas NO conversion increased up to 74% for the 1.9% Cu/SAPO-34 catalyst prepared by SSIE. This behavior can be explained by different copper species present in catalysts prepared by both methodologies and attending to the recently proposed fast NH_3-SCR reaction mechanism,[7] which claims that the key step is the formation of a NO_2 molecule in the gas

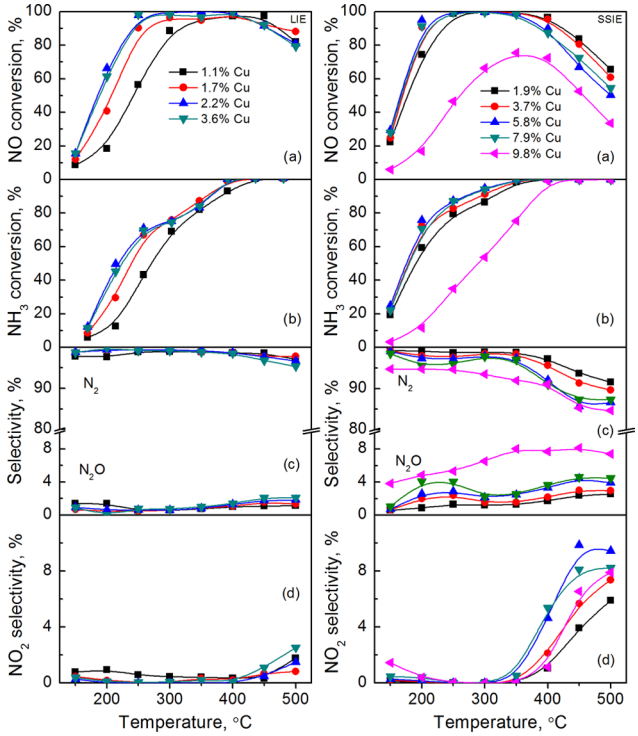

Figure 10. Evaluation of NH_3-SCR performance for samples prepared by LIE and SSIE with different copper loadings. (a) NO conversion, (b) NH_3 conversion, (c) N_2 and N_2O selectivities, and (d) NO_2 selectivity.

DOI: 10.1021/acsomega.9b01118
ACS Omega 2019, 4, 14699−14713

phase. The formation of NO_2 could occur by two reaction paths: (i) reaction of NO with an adsorbed nitrate specie, leaving an adsorbed nitrite specie, which then reacts with NH_3 to form N_2 and H_2O (note that adsorbed nitrites and nitrates have been detected by FTIR during the NH_3-SCR reaction),[65,66] and (ii) direct oxidation of NO with O_2 over Cu sites. Verma et al.[67] found that the NO oxidation rate per mol of Cu was higher in the presence of Cu_xO_y species rather than isolated copper ions. Thus, the higher NH_3-SCR activity for the SSIE preparation methodology can be linked to the higher oxidation capacity of the catalyst due to the preferential formation of copper aggregates and clusters, which can catalyze the oxidation of NO to NO_2 readily at low temperatures and activate the fast NH_3-SCR reaction ($2NH_3 + NO + NO_2 \rightarrow 2N_2 + 3H_2O$). On the other hand, copper ions are the main copper species for catalysts prepared by LIE, specifically those with low copper loading. Copper ions are not so active in catalyzing the oxidation of NO to NO_2,[67] and consequently in the absence of gas-phase NO_2, the fast SCR is not running and the reaction proceeds through the standard SCR ($4NH_3 + 4NO + O_2 \rightarrow 4N_2 + 6H_2O$), which is known to be slower than the fast SCR.[68]

Copper species also presented an important impact on high-temperature NH_3-SCR activity. The promotion of the oxidation capacity for SSIE catalysts due to the presence of copper aggregates and clusters implies some other drawbacks, such as NH_3 oxidation starts becoming significant at intermediate temperatures and thus the high-temperature NH_3-SCR activity is penalized. On the other hand, catalysts prepared by LIE presented better high-temperature NH_3-SCR activity due to the preferential formation of Cu^{2+} ions with lower oxidation capacity.

The higher oxidation ability of samples prepared by SSIE is evidenced by a higher selectivity to NO_2 at high temperatures. Focusing on product selectivity, it can be observed that samples prepared by LIE presented higher nitrogen selectivity than SSIE, irrespective of copper loading.

The NH_3-SCR reaction activation energies for samples prepared by LIE and SSIE with different copper loadings (Figure S6) were calculated from experiments carried out at differential reactor regimes. Calculated reaction rate, activation energy, and TOF have been listed in Tables S4 and S5. The activation energy was situated around 40−47 kJ mol^{-1} for samples prepared by LIE, whereas slightly lower values were observed for SSIE, around 32−38 kJ mol^{-1}. This difference can be related to different mechanisms running during the NH_3-SCR. As already explained, the higher oxidation capacity of SSIE catalysts promotes oxidation of NO to NO_2 and thus activates the fast NH_3-SCR, which would not be running for LIE catalysts due to their lower oxidation capacity. Specifically, the sample prepared by LIE with a copper loading of 1.1% presented a notably lower activation energy, i.e., 19 kJ mol^{-1}, which could be as a consequence of a different reaction mechanism due to such a low copper content.

Finally, Figure 11 shows the reaction rate normalized per mol of copper, $-r_{NO}$ (mol NO (mol Cu)$^{-1}$ s^{-1}), and turnover frequency (TOF) values at 200 °C for samples prepared by LIE and SSIE. Focusing on samples prepared by LIE, a clear decrease of the reaction rate ($-r_{NO}$) can be observed with increasing copper loading. This fact can be explained by a progressive increase in the proportion of copper aggregates with respect to copper ions. On the other hand, similar TOF values are obtained irrespective of copper loading, i.e., 12 × 10^{-3} s^{-1}, which again evidences that copper ions are the main active site for NH_3-SCR. Regarding SSIE catalysts, a decreasing tendency of the reaction rate ($-r_{NO}$) is also observed, which again can be correlated with a higher proportion of copper aggregates as copper loading is increased. Contrary to samples prepared by LIE, a decreasing tendency in TOF values is still evident as copper loading is increased for SSIE samples, specifically for samples with copper loading above 8%. This fact is attributed to a notably lower specific surface area and acidity of those samples (Table 3). Precise comparison among TOF values obtained by other works is not straightforward because the reaction conditions differ from each other. For example, Xue et al.[16] found a TOF of 42 × 10^{-3} s^{-1} at 200 °C using the Cu-SAPO-34 catalyst and a feedstream composed of 500 ppm NO, 500 ppm NH_3, and 5% O_2 with N_2 as the balance gas. Hu et al.[49] determined a TOF value of 11 × 10^{-3} s^{-1} at 200 °C using Cu-SAPO-34 and the same feedstream composition. The maximum TOF values observed in the present study are 18 × 10^{-3} and 24 × 10^{-3} s^{-1} for LIE and SSIE methodologies, respectively. These values lie between the aforementioned TOF values determined by other authors. Figure 11 also includes two additional samples prepared by ion exchanging the H/SAPO-34 with NH_4NO_3 to obtain NH_4/SAPO-34 prior to the copper incorporation by LIE and eliminating the intermediate ion exchange with Na. Then, a fraction of the prepared sample was calcined at 500 °C and the other at 700 °C. The copper loading of the prepared catalysts was 2.1%.

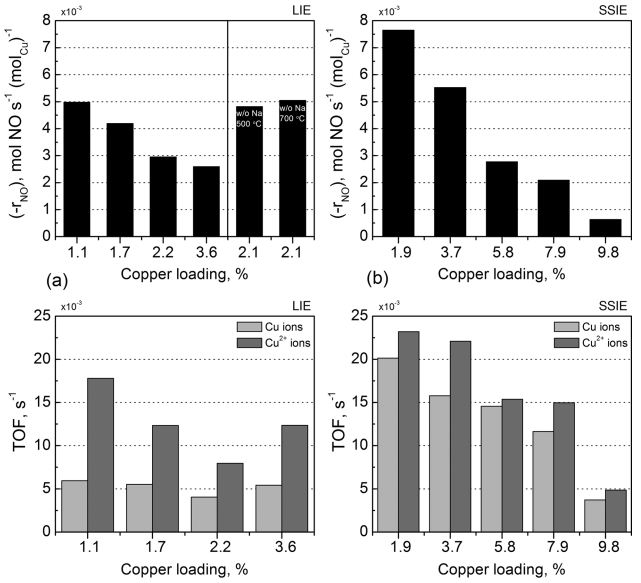

Figure 11. Evolution of the reaction rate and the turnover frequency as a function of copper loading for samples prepared by LIE (a) and SSIE (b). TOF values are referred to the total amount of copper ions or alternatively to the amount of Cu^{2+} ions quantified by H_2-TPR.

The presence of residual alkali or alkaline earth cocations on the activity of NH_3-SCR is not clear in the literature, as some authors claimed a beneficial effect,[69] whereas others claimed a detrimental effect for high contents.[70] The prepared LIE catalyst presented a Na content of around 0.25%, irrespective of the copper loading, whereas in the absence of Na ion exchange, the Na content was below the detection limit of the XRF technique (<0.05%). As can be observed in Figure 11, in the absence of residual Na cocations, the reaction rate value is increased up to 4.8 × 10^{-3} s^{-1}, whereas in the presence of

DOI: 10.1021/acsomega.9b01118
ACS Omega 2019, 4, 14699−14713

residual Na, the $(-r_{NO})$ is 3×10^{-3} s^{-1}. Thus, it can be concluded that the presence of residual Na cocations limits the activity of Cu/SAPO-34 to some extent.

Then, the reaction rate of the Cu/SAPO-34 catalyst prepared in the absence of Na ion exchange and calcined at the same calcination temperature as SSIE, i.e., 700 °C, was also compared (Figure 11a). As can be observed, the temperature increase during the calcination step from 500 up to 700 °C hardly affected the reaction rate, slightly increasing from 4.8×10^{-3} to 5.1×10^{-3} s^{-1}. Thus, it seems that a temperature increase during the calcination step of Cu/SAPO-34 catalysts prepared by LIE in the absence of Na cocations does not critically affect the nature of copper species and thus the NH_3-SCR activity is maintained constant.

The TOF has been calculated based on the amount of total copper ions (Cu^{2+} and Cu^{+}) or exclusively based on the amount of Cu^{2+} ions. The TOF of catalysts prepared by LIE differs notably when referred to the amount of total copper ions or Cu^{2+}, as the amount of Cu^{+} ions is notable (Table 4). Differences in TOF are not so noteworthy for catalysts prepared by SSIE due to the lower amount of Cu^{+} ions. Using the TOF referred to the amount of Cu^{2+} ions, it can be observed that the TOF for the catalyst prepared by SSIE with a copper loading of 1.9% is 23.2×10^{-3} s^{-1}, which is notably higher than the TOF calculated for the catalyst prepared by LIE with a copper loading of 1.7%, i.e., 12.3×10^{-3} s^{-1}. Thus, the SSIE procedure achieves higher activity per Cu^{2+} site, which enhances NH_3-SCR activity.

■ ASSOCIATED CONTENT

Supporting Information

The Supporting Information is available free of charge on the ACS Publications website at DOI: 10.1021/acsomega.9b01118.

Detailed information on physicochemical properties of all prepared SSIE and LIE samples, as well as catalytic behavior of prepared catalysts in the NO_x NH_3-SCR reaction and determination of reaction rates and activation energies (PDF)

■ AUTHOR INFORMATION

Corresponding Author

*E-mail: juanra.gonzalezvelasco@ehu.es.

ORCID

Juan R. González-Velasco: 0000-0002-8679-1805

Notes

The authors declare no competing financial interest.

■ ACKNOWLEDGMENTS

The authors wish to acknowledge the financial support provided by the Spanish Economy and Competitiveness Ministry (CTQ2015-67597-2-1-R) and the Basque Government (IT657-013 and IT1297-19). Also, technical support by SGIker (UPV/EHU Advanced Research Facilities) is acknowledged. The assistance of Prof. Luis Lezama during EPR analysis and interpretation is gratefully acknowledged. U.D.-L.-T. and M.U. want to acknowledge UPV/EHU and the Spanish Economy and Competitiveness for the postdoc (ESPDOC16/69) and Ph.D. (BFI-2010-330) research grants, respectively.

■ REFERENCES

(1) Epling, W. S.; Campbell, L. E.; Yezerets, A.; Currier, N. W.; Parks, J. E. Overview of the fundamental reactions and degradation mechanisms of NO_x storage/reduction catalysts. *Catal. Rev.* **2004**, *46*, 163−245.

(2) Koebel, M.; Elsener, M.; Kleemann, M. Urea-SCR: a promising technique to reduce NO_x emissions from automotive diesel engines. *Catal. Today* **2000**, *59*, 335−345.

(3) Brandenberger, S.; Kroecher, O.; Tissler, A.; Althoff, R. The State of the Art in Selective Catalytic Reduction of NO_x by Ammonia Using Metal-Exchanged Zeolite Catalysts. *Catal. Rev.* **2008**, *50*, 492−531.

(4) Xu, L.; McCabe, R. W. LNT+in situ SCR catalyst system for diesel emissions control. *Catal. Today* **2012**, *184*, 83−94.

(5) Yim, S. D.; Kim, S. J.; Baik, J. H.; Nam, I. S.; Mok, Y. S.; Lee, J. H.; Cho, B. K.; Oh, S. H. Decomposition of Urea into NH_3 for the SCR Process. *Ind. Eng. Chem. Res.* **2004**, *43*, 4856−4863.

(6) De-La-Torre, U.; Pereda-Ayo, B.; Gutiérrez-Ortiz, M. A.; González-Marcos, J. A.; González-Velasco, J. R. Steady-state NH_3-SCR global model and kinetic parameter estimation for NO_x removal in diesel engine exhaust aftertreatment with Cu/chabazite. *Catal. Today* **2017**, *296*, 95−104.

(7) Janssens, T. V. W.; Falsig, H.; Lundegaard, L. F.; Vennestrom, P. N. R.; Rasmussen, S. B.; Moses, P. G.; Giordanino, F.; Borfecchia, E.; Lomachenko, K. A.; Lamberti, C.; Bordiga, S.; Godiksen, A.; Mossin, S.; Beato, P. A Consistent Reaction Scheme for the Selective Catalytic Reduction of Nitrogen Oxides with Ammonia. *ACS Catal.* **2015**, *5*, 2832−2845.

(8) Li, J.; Chang, H.; Ma, L.; Hao, J.; Yang, R. T. Low-temperature selective catalytic reduction of NO_x with NH_3 over metal oxide and zeolite catalysts—A review. *Catal. Today* **2011**, *175*, 147−156.

(9) De-La-Torre, U.; Pereda-Ayo, B.; Moliner, M.; González-Velasco, J. R.; Corma, A. Cu-zeolite catalysts for NO_x removal by selective catalytic reduction with NH_3 and coupled to NO storage/reduction monolith in diesel engine exhaust aftertreatment systems. *Appl. Catal., B* **2016**, *187*, 419−427.

(10) Martens, J. A.; Mertens, M.; Grobet, P. J.; Jacobs, P. A. In *Synthesis and Characterization of Silicon-Rich SAPO-5*; Grobet, P. J., Ed.; Studies in Surface Science and Catalysis; Elsevier: Amsterdam, 1988; Vol. *37*, pp 97−105.

(11) Clemens, A. K. S.; Shishkin, A.; Carlsson, P. A.; Skoglundh, M.; Martinez-Casado, F. J.; Matej, Z.; Balmes, O.; Harelind, H. Reaction-driven Ion Exchange of Copper into Zeolite SSZ-13. *ACS Catal.* **2015**, *5*, 6209−6218.

(12) Shwan, S.; Skoglundh, M.; Lundegaard, L. F.; Tiruvalam, R. R.; Janssens, T. V. W.; Carlsson, A.; Vennestrom, P. N. R. Solid-State Ion-Exchange of Copper into Zeolites Facilitated by Ammonia at Low Temperature. *ACS Catal.* **2015**, *5*, 16−19.

(13) Gao, F.; Walter, E. D.; Washton, N. M.; Szanyi, J.; Peden, C. H. F. Synthesis and evaluation of Cu/SAPO-34 catalysts for NH_3-SCR 2: Solid-state ion exchange and one-pot synthesis. *Appl. Catal., B* **2015**, *162*, 501−514.

(14) Wang, D.; Gao, F.; Peden, C. H. F.; Li, J.; Kamasamudram, K.; Epling, W. S. Selective Catalytic Reduction of NO_x with NH_3 over a Cu-SSZ-13 Catalyst Prepared by a Solid-State Ion-Exchange Method. *ChemCatChem* **2014**, *6*, 1579−1583.

(15) Wang, J.; Zhao, H.; Haller, G.; Li, Y. Recent advances in the selective catalytic reduction of NO_x with NH_3 on Cu-Chabazite Catalysts. *Appl. Catal., B* **2017**, *202*, 346−354.

(16) Xue, J.; Wang, X.; Qi, G.; Wang, J.; Shen, M.; Li, W. Characterization of copper species over Cu/SAPO-34 in selective catalytic reduction of NO_x with ammonia: Relationships between active Cu sites and de-NO_x performance at low temperature. *J. Catal.* **2013**, *297*, 56−64.

(17) Kwak, J. H.; Tran, D.; Burton, S. D.; Szanyi, J.; Lee, J. H.; Peden, C. H. F. Effects of hydrothermal aging on NH_3-SCR reaction over Cu/zeolites. *J. Catal.* **2012**, *287*, 203−209.

DOI: 10.1021/acsomega.9b01118
ACS Omega 2019, 4, 14699−14713

(18) Ma, J.; Si, Z.; Weng, D.; Wu, X.; Ma, Y. Potassium poisoning on Cu/SAPO-34 catalyst for selective catalytic reduction of NO_x with ammonia. *Chem. Eng. J.* **2015**, *267*, 191−200.
(19) Yu, T.; Hao, T.; Fan, D.; Wang, J.; Shen, M.; Li, W. Recent NH_3-SCR Mechanism Research over Cu/SAPO-34 Catalyst. *J. Phys. Chem. C* **2014**, *118*, 6565−6575.
(20) Frache, A.; Palella, B.; Cadoni, M.; Pirone, R.; Ciambelli, P.; Pastore, H. O.; Marchese, L. Catalytic $DeNO_x$ activity of cobalt and copper ions in microporous MeALPO-34 and MeAPSO-34. *Catal. Today* **2002**, *75*, 359−365.
(21) Wang, L.; Gaudet, J. R.; Li, W.; Weng, D. Migration of Cu species in Cu/SAPO-34 during hydrothermal aging. *J. Catal.* **2013**, *306*, 68−77.
(22) Giordanino, F.; Vennestrøm, P. N. R.; Lundegaard, L. F.; Stappen, F. N.; Mossin, S.; Beato, P.; Bordiga, S.; Lamberti, C. Characterization of Cu-exchanged SSZ-13: a comparative FTIR, UV-Vis, and EPR study with Cu-ZSM-5 and Cu-β with similar Si/Al and Cu/Al ratios. *Dalton Trans.* **2013**, *42*, 12741−12761.
(23) Gao, F.; Walter, E. D.; Kollar, M.; Wang, Y.; Szanyi, J.; Peden, C. H. F. Understanding ammonia selective catalytic reduction kinetics over Cu/SSZ-13 from motion of the Cu ions. *J. Catal.* **2014**, *319*, 1−14.
(24) Gao, F.; Walter, E. D.; Karp, E. M.; Luo, J.; Tonkyn, R. G.; Kwak, J. H.; Szanyi, J.; Peden, C. H. F. Structure−activity relationships in NH_3-SCR over Cu-SSZ-13 as probed by reaction kinetics and EPR studies. *J. Catal.* **2013**, *300*, 20−29.
(25) Yu, T.; Wang, J.; Shen, M.; Li, W. NH_3-SCR over Cu/SAPO-34 catalysts with various acid contents and low Cu loading. *Catal. Sci. Technol.* **2013**, *3*, 3234−3241.
(26) Kucherov, A. V.; Hubbard, C. P.; Kucherova, T. N.; Shelef, M. Stabilization of the ethane oxidation catalytic activity of Cu-ZSM-5. *Appl. Catal., B* **1996**, *7*, 285−298.
(27) Beale, A. M.; Gao, F.; Lezcano-Gonzalez, I.; Peden, C. H. F.; Szanyi, J. Recent advances in automotive catalysis for NO_x emission control by small-pore microporous materials. *Chem. Soc. Rev.* **2015**, *44*, 7371−7405.
(28) Dzwigaj, S.; Stievano, L.; Wagner, F. E.; Che, M. Effect of preparation and metal content on the introduction of Fe in BEA zeolite, studied by DR UV−vis, EPR and Mössbauer spectroscopy. *J. Phys. Chem. Solids* **2007**, *68*, 1885−1891.
(29) Zhilinskaya, E. A.; Delahay, G.; Mauvezin, M.; Coq, B.; Aboukais, A. EPR Investigation of Fe-Exchanged Beta-Zeolites. *Langmuir* **2003**, *19*, 3596−3602.
(30) Sultana, A.; Nanba, T.; Haneda, M.; Sasaki, M.; Hamada, H. Influence of cocations on the formation of Cu^+ species in Cu/ZSM-5 and its effect on selective catalytic reduction of NO_x with NH_3. *Appl. Catal., B* **2010**, *101*, 61−67.
(31) Torre-Abreu, C.; Ribeiro, M. F.; Henriques, C.; Delahay, G. Characterisation of CuMFI catalysts by temperature programmed desorption of NO and temperature programmed reduction. Effect of the zeolite Si/Al ratio and copper loading. *Appl. Catal., B* **1997**, *12*, 249−262.
(32) Richter, M.; Fait, M. J. G.; Eckelt, R.; Schreier, E.; Schneider, M.; Pohl, M. M.; Fricke, R. Oxidative gas phase carbonylation of methanol to dimethyl carbonate over chloride-free Cu-impregnated zeolite Y catalysts at elevated pressure. *Appl. Catal., B* **2007**, *73*, 269−281.
(33) Wang, D.; Zhang, L.; Li, J.; Kamasamudram, K.; Epling, W. S. NH_3-SCR over Cu/SAPO-34−Zeolite acidity and Cu structure changes as a function of Cu Loading. *Catal. Today* **2014**, *231*, 64−74.
(34) Zhang, T.; Qiu, F.; Chang, H.; Li, X.; Li, J. Identification of active sites and reaction mechanism on low-temperature SCR activity over Cu-SSZ-13 catalysts prepared by different methods. *Catal. Sci. Technol.* **2016**, *6*, 6294−6304.
(35) Deka, U.; Lezcano-Gonzalez, I.; Warrender, S. J.; Lorena Picone, A.; Wright, P. A.; Weckhuysen, B. M.; Beale, A. M. Changing active sites in Cu−CHA catalysts: $deNO_x$ selectivity as a function of the preparation method. *Microporous Mesoporous Mater.* **2013**, *166*, 144−152.
(36) Liu, X.; Wu, X.; Weng, D.; Si, Z.; Ran, R. Evolution of copper species on Cu/SAPO-34 SCR catalysts upon hydrothermal aging. *Catal. Today* **2017**, *281*, 596−604.
(37) Ming, S.; Chen, Z.; Fan, C.; Pang, L.; Guo, W.; Albert, K. B. B.; Liu, P.; Li, T. The effect of copper loading and silicon content on catalytic activity and hydrothermal stability of Cu-SAPO-18 catalyst for NH_3-SCR. *Appl. Catal., A* **2018**, *559*, 47−56.
(38) Peng, B.; Feng, C.; Liu, S.; Zhang, R. Synthesis of CuO catalyst derived from HKUST-1 temple for the low-temperature NH_3-SCR process. *Catal. Today* **2018**, *314*, 122−128.
(39) Han, S.; Ye, Q.; Cheng, S.; Kang, T.; Dai, H. Effect of the hydrothermal aging temperature and Cu/Al ratio on the hydrothermal stability of CuSSZ-13 catalysts for NH3-SCR. *Catal. Sci. Technol.* **2017**, *7*, 703−717.
(40) Lezcano-Gonzalez, I.; Deka, U.; Arstad, B.; Van Yperen-De Deyne, A.; Hemelsoet, K.; Waroquier, M.; Van Speybroeck, V.; Weckhuysen, B. M.; Beale, A. M. Determining the storage, availability and reactivity of NH_3 within Cu-Chabazite-based Ammonia Selective Catalytic Reduction systems. *Phys. Chem. Chem. Phys.* **2014**, *16*, 1639−1650.
(41) Martínez-Franco, R.; Moliner, M.; Franch, C.; Kustov, A.; Corma, A. Rational direct synthesis methodology of very active and hydrothermally stable Cu-SAPO-34 molecular sieves for the SCR of NO_x. *Appl. Catal., B* **2012**, *127*, 273−280.
(42) Cortés-Reyes, M.; Finocchio, E.; Herrera, C.; Larrubia, M. A.; Alemany, L. J.; Busca, G. A study of Cu-SAPO-34 catalysts for SCR of NO_x by ammonia. *Microporous Mesoporous Mater.* **2017**, *241*, 258−265.
(43) Dang, T. T. H.; Zubowa, H.; Bentrup, U.; Richter, M.; Martin, A. Microwave-assisted synthesis and characterization of Cu-containing $AlPO_4$-5 and SAPO-5. *Microporous Mesoporous Mater.* **2009**, *123*, 209−220.
(44) Pestryakov, A. N.; Petranovskii, V. P.; Kryazhov, A.; Ozhereliev, O.; Pfander, N.; Knop-Gericke, A. Study of copper nanoparticles formation on supports of different nature by UV−Vis diffuse reflectance spectroscopy. *Chem. Phys. Lett.* **2004**, *385*, 173−176.
(45) Kecht, J.; Tahri, Z.; De Waele, V.; Mostafavi, M.; Mintova, S.; Bein, T. Colloidal Zeolites as Host Matrix for Copper Nanoclusters. *Chem. Mater.* **2006**, *18*, 3373−3380.
(46) De La Torre, U.; Pereda-Ayo, B.; González-Velasco, J. R. Cu-zeolite NH_3-SCR catalysts for NO_x removal in the combined NSR−SCR technology. *Chem. Eng. J.* **2012**, *207−208*, 10−17.
(47) Ciardelli, C.; Nova, I.; Tronconi, E.; Chatterjee, D.; Bandl-Konrad, B.; Weibel, M.; Krutzsch, B. Reactivity of NO/NO_2−NH_3 SCR system for diesel exhaust aftertreatment: Identification of the reaction network as a function of temperature and NO_2 feed content. *Appl. Catal., B* **2007**, *70*, 80−90.
(48) Colombo, M.; Nova, I.; Tronconi, E. Detailed kinetic modeling of the NH_3−NO/NO_2 SCR reactions over a commercial Cu-zeolite catalyst for Diesel exhausts after treatment. *Catal. Today* **2012**, *197*, 243−255.
(49) Hu, X.; Yang, M.; Fan, D.; Qi, G.; Wang, J.; Wang, J.; Yu, T.; Li, W.; Shen, M. The role of pore diffusion in determining NH_3 SCR active sites over Cu/SAPO-34 catalysts. *J. Catal.* **2016**, *341*, 55−61.
(50) Wang, J.; Fan, D.; Yu, T.; Wang, J.; Hao, T.; Hu, X.; Shen, M.; Li, W. Improvement of low-temperature hydrothermal stability of Cu/SAPO-34 catalysts by Cu^{2+} species. *J. Catal.* **2015**, *322*, 84−90.
(51) Yu, T.; Fan, D.; Hao, T.; Wang, J.; Shen, M.; Li, W. The effect of various templates on the NH_3-SCR activities over Cu/SAPO-34 catalysts. *Chem. Eng. J.* **2014**, *243*, 159−168.
(52) Chen, L.; Jansson, J.; Skoglundh, M.; Grönbeck, H. Mechanism for Solid-State Ion Exchange of Cu+ into Zeolites. *J. Phys. Chem. C* **2016**, *120*, 29182−29189.
(53) Paolucci, C.; Khurana, I.; Parekh, A. A.; Li, S.; Shih, A. J.; Li, H.; Di Iorio, J. R.; Albarracin-Caballero, J. D.; Yezerets, A.; Miller, J. T.; Delgass, W. N.; Ribeiro, F. H.; Schneider, W. F.; Gounder, R. Dynamic multinuclear sites formed by mobilized copper ions in NOx selective catalytic reduction. *Science* **2017**, *357*, 898−903.

DOI: 10.1021/acsomega.9b01118
ACS Omega 2019, 4, 14699−14713

(54) Fickel, D. W.; Lobo, R. F. Copper Coordination in Cu-SSZ-13 and Cu-SSZ-16 Investigated by Variable-Temperature XRD. *J. Phys. Chem. C* **2010**, *114*, 1633−1640.
(55) Deka, U.; Juhin, A.; Eilertsen, E. A.; Emerich, H.; Green, M. A.; Korhonen, S. T.; Weckhuysen, B. M.; Beale, A. M. Confirmation of Isolated Cu^{2+} Ions in SSZ-13 Zeolite as Active Sites in NH3-Selective Catalytic Reduction. *J. Phys. Chem. C* **2012**, *116*, 4809−4818.
(56) Gao, F.; Wang, Y.; Washton, N. M.; Kollar, M.; Szanyi, J.; Peden, C. H. F. Effects of Alkali and Alkaline Earth Cocations on the Activity and Hydrothermal Stability of Cu/SSZ-13 NH_3−SCR Catalysts. *ACS Catal.* **2015**, *5*, 6780−6791.
(57) Wang, L.; Li, W.; Qi, G.; Weng, D. Location and nature of Cu species in Cu/SAPO-34 for selective catalytic reduction of NO with NH_3. *J. Catal.* **2012**, *289*, 21−29.
(58) Wang, J.; Huang, Y.; Yu, T.; Zhu, S.; Shen, M.; Li, W.; Wang, J. The migration of Cu species over Cu−SAPO-34 and its effect on NH_3 oxidation at high temperature. *Catal. Sci. Technol.* **2014**, *4*, 3004−3012.
(59) Beale, A. M.; Lezcano-Gonzalez, I.; Slawinksi, W. A.; Wragg, D. S. Correlation between Cu ion migration behavior and deNO_x activity in Cu-SSZ-13 for the standard NH_3-SCR reaction. *Chem. Commun.* **2016**, *52*, 6170−6173.
(60) Chen, P.; Khetan, A.; Jablonska, M.; Simböck, J.; Muhler, M.; Palkovits, R.; Pitsch, H.; Simon, U. Local dynamics of copper active sites in zeolite catalysts for selective catalytic reduction of NO_x with NH_3. *Appl. Catal., B* **2018**, *237*, 263−272.
(61) Borfecchia, E.; Lomachenko, K. A.; Giordanino, F.; Falsig, H.; Beato, P.; Soldatov, A. V.; Bordiga, S.; Lamberti, C. Revisiting the nature of Cu sites in the activated Cu-SSZ-13 catalyst for SCR reaction. *Chem. Sci.* **2015**, *6*, 548−563.
(62) Dong, X.; Wang, J.; Zhao, H.; Li, Y. The promotion effect of CeO_x on Cu-SAPO-34 catalyst for selective catalytic reduction of NO_x with ammonia. *Catal. Today* **2015**, *258*, 28−34.
(63) Kefirov, R.; Penkova, A.; Hadjiivanov, K.; Dzwigaj, S.; Che, M. Stabilization of Cu^+ ions in BEA zeolite: Study by FTIR spectroscopy of adsorbed CO and TPR. *Microporous Mesoporous Mater.* **2008**, *116*, 180−187.
(64) Pereda-Ayo, B.; De La Torre, U.; Illán-Gómez, M. J.; Bueno-López, A.; González-Velasco, J. R. Role of the different copper species on the activity of Cu/zeolite catalysts for SCR of NO_x with NH_3. *Appl. Catal., B* **2014**, *147*, 420−428.
(65) Ruggeri, M. P.; Selleri, T.; Colombo, M.; Nova, I.; Tronconi, E. Identification of nitrites/HONO as primary products of NO oxidation over Fe-ZSM-5 and their role in the Standard SCR mechanism: A chemical trapping study. *J. Catal.* **2014**, *311*, 266−270.
(66) Grossale, A.; Nova, I.; Tronconi, E. Role of Nitrate Species in the "NO_2-SCR" Mechanism over a Commercial Fe-zeolite Catalyst for SCR Mobile Applications. *Catal. Lett.* **2009**, *130*, 525−531.
(67) Verma, A. A.; Bates, S. A.; Anggara, T.; Paolucci, C.; Parekh, A. A.; Kamasamudram, K.; Yezerets, A.; Miller, J. T.; Delgass, W. N.; Schneider, W. F.; Ribeiro, F. H. NO oxidation: A probe reaction on Cu-SSZ-13. *J. Catal.* **2014**, *312*, 179−190.
(68) Kato, A.; Matsuda, S.; Kamo, T.; Nakajima, F.; Kuroda, H.; Narita, T. Reaction between nitrogen oxide (NO_x) and ammonia on iron oxide-titanium oxide catalyst. *J. Phys. Chem. A* **1981**, *85*, 4099−4102.
(69) Zhao, Z.; Yu, R.; Zhao, R.; Shi, C.; Gies, H.; Xiao, F. S.; Vos, D. D.; Yokoi, T.; Bao, X.; Kolb, U.; Feyen, M.; McGuire, R.; Maurer, S.; Moini, A.; Müller, U.; Zhang, W. Cu-exchanged Al-rich SSZ-13 zeolite from organotemplate-free synthesis as NH_3-SCR catalyst: Effects of Na^+ ions on the activity and hydrothermal stability. *Appl. Catal., B* **2017**, *217*, 421−428.
(70) Xie, L.; Liu, F.; Shi, X.; Xiao, F. S.; He, H. Effects of post-treatment method and Na co-cation on the hydrothermal stability of Cu−SSZ-13 catalyst for the selective catalytic reduction of NO_x with NH_3. *Appl. Catal., B* **2015**, *179*, 206−212.

DOI: 10.1021/acsomega.9b01118
ACS Omega 2019, 4, 14699−14713